

# Denoising Diffusion Probabilistic Models for Hardware-Impaired Communication Systems: Towards Wireless Generative AI

Mehdi Letafati, *Student Member, IEEE*, Samad Ali, *Member, IEEE*, and Matti Latva-aho, *Senior Member, IEEE*

**Abstract**—Thanks to the outstanding achievements from state-of-the-art generative models like ChatGPT and diffusion models, generative AI has gained substantial attention across various industrial and academic domains. In this paper, denoising diffusion probabilistic models (DDPMs) are proposed for a practical finite-precision wireless communication system with hardware-impaired transceivers. The intuition behind DDPM is to decompose the data generation process over the so-called “denoising” steps. Inspired by this, a DDPM-based receiver is proposed for a practical wireless communication scheme that faces realistic non-idealities, including hardware impairments (HWI), channel distortions, and quantization errors. It is shown that our approach provides *network resilience* under low-SNR regimes, *near-invariant* reconstruction performance with respect to different HWI levels and quantization errors, and robust *out-of-distribution performance* against non-Gaussian noise. Moreover, the reconstruction performance of our scheme is evaluated in terms of cosine similarity and mean-squared error (MSE), highlighting more than 25 dB improvement compared to the conventional deep neural network (DNN)-based receivers.

**Index Terms**—AI-native wireless, diffusion models, generative AI, network resilience, wireless AI, denoising diffusions.

## I. INTRODUCTION

### A. Motivation & Background

With the emergence of deep generative models, the realm of artificial intelligence (AI) has witnessed a paradigm shift towards the novel concept of generative AI that can facilitate the development of AI-based systems [2]. At the same time, from data communication and networking perspective, “connected intelligence” is envisioned as the most significant driving force in the sixth generation (6G) of communications—AI and machine learning (AI/ML) algorithms are envisioned to be widely incorporated into 6G wireless networks, realizing “AI-native” communication systems [3]–[6]. This underscores the need for novel AI/ML-based solutions to be tailored to meet the requirements of emerging communication scenarios.

The evolution of diffusion models [7], as the new paradigm in deep generative models, can be regarded as one of the main factors contributing to the recent breakthroughs in generative AI, that have already showcased notable success with some of the popular examples such as DALL·E 2 by OpenAI,<sup>1</sup> and ImageGen by Google Brain.<sup>2</sup> Diffusion models have

realized unprecedented results in different applications, such as computer vision, natural language processing (NLP), data analysis and synthesis, and medical imaging [8]. Please see [9] and references therein for a comprehensive survey on diffusion models.

The core concept of diffusion modelling is that if we could develop an ML model that is capable of learning the *systematic decay of information*, due to noise/distortions, then it should be possible to “reverse” the process and recover the information back from the noisy/erroneous data. This is fundamentally different from conventional generative models, like generative adversarial networks (GANs) and variational autoencoders (VAEs). While GANs try to directly learn the distribution of highly-structured data, and VAEs’ objective is to learn a low-dimensional latent space representation, a diffusion model is comprised of two processes, i.e., the forward diffusion process and the parametric reverse process. Within the forward process, random noise is purposefully added to the original data, and then, the reverse process is run to “decode” and generate samples from noise. Accordingly, the close underlying relation between the key concepts on how diffusion models work and the problems in wireless communication systems has motivated us to carry out this research.

### B. Related Works

Ongoing research on diffusion models encompasses both theoretical advancements and practical applications across different domains of computer science. However, there have been only a few papers in wireless communication literature that have started looking into the potential merits of diffusion-based generative models for wireless systems [10]–[16]. Notably, the incorporation of diffusion models into wireless communication problems is still in its infancy, and we hope that this paper would shed light on one of the applications of diffusion models for wireless systems.

To provide the literature review, the authors in [10] study a workflow for utilizing diffusion models in wireless network management. They study the incentive mechanisms for generating contracts using diffusion models in mobile AI-generated content services. They exploit the exploration capability of diffusion models in Q-learning algorithms for network management. Denoising diffusion model is utilized in [11] to generate synthetic channel realizations conditioned on the message information. The authors tackle the problem of differentiable channel model within the gradient-based training process of end-to-end ML-based communications.

Preliminary results of this paper are submitted to the IEEE Wireless Communications and Networking Conference (WCNC 2024), Dubai, United Arab Emirates, Apr. 2024 [1].

The authors are with the Centre for Wireless Communications, University of Oulu, Oulu, Finland (e-mails: mehdi.letafati@oulu.fi; samad.ali@oulu.fi; matti.latva-aho@oulu.fi).

<sup>1</sup><https://openai.com/dall-e-2>

<sup>2</sup><https://imagen.research.google/>

The results highlight the performance of diffusion models as an alternative to generative adversarial network (GAN)-based schemes. It is shown in [11] that GANs experience unstable training and less diversity in generation performance, due to their adversarial training nature. However, diffusion models maintain a more stable training process and a better generalization during inference. Noise-conditioned score network (NCSN)-based channel estimation is studied in [12] and [13] for multi-input-multi-output (MIMO) wireless communication scenario. The authors estimate the gradient of the high-dimensional log-prior of wireless channels, using RefineNet neural network architecture [17] comprised of 24 hidden channels in the first layer and a depth of six residual blocks in both the encoder and decoder parts. Posterior sampling method is further applied to make the generated channel estimations consistent with the pilot signals measured at the receiver. The results in [12] and [13] highlight a competitive performance for both in- and out-of-distribution (OOD) scenarios compared to GANs and compressed sensing methods, without the need for any online fine-tuning. In [14], deep learning-based joint source-channel coding (Deep-JSCC) is combined with diffusion models to complement digital communication schemes with a generative component. The results of this “hybrid” scheme indicate that the perceptual quality of reconstruction can be improved when employing diffusion models. Recently, we have proposed a novel scheme for probabilistic constellation shaping using diffusion models [15]. The results show a significant performance gain compared to deep neural network (DNN)-based schemes, with a threefold improvement in terms of mutual information metric.

Despite the close relation between the underlying mechanism of diffusion models and what is essentially expected from the receiver of a communication system to denoise, decode, and reconstruct the information signals from the noisy and distorted received signals, to the best of our knowledge, there is only one preprint [16] that studies the application of denoising diffusion models in wireless to help improve the receiver’s performance in terms of noise removal. The authors utilize denoising diffusion models and call it channel denoising diffusion model (CDDM). However, the paper has some drawbacks which need further considerations. To elaborate, i) the paper does not provide a comprehensive study on the potential capabilities of diffusion models in alleviating different factors that affect communication systems. Specifically, the authors do not evaluate the performance of their CDDM module under realistic scenarios such as transceiver impairments, low-SNR regimes, non-Gaussian noise, and quantization effects, and their goal is to simply compensate for the receiver noise due to the receiver noise and channel equalization errors. ii) Although diffusion models have shown promising performance in generating samples from structured data distributions, the authors implement another neural decoder block at the receiver, in addition to CDDM. However, having two different ML models, each maintaining a distinct objective function (while their optimization also depends on each other) can impose computational overhead to the network. iii) The proposed scheme in [16] relies on the

channel state information (CSI) knowledge at the diffusion module—the transmitter, e.g., the base station in downlink data transmission, has to feed back the CSI data to the receiver, which can cause communication overhead and might not be aligned with communication standards.

### C. Our Contributions

In this paper, we propose denoising diffusion probabilistic models (DDPM), as a new state-of-the-art family of generative models proposed by Ho *et al.* in 2020 [7], for a practical point-to-point communication system with finite precision transmission and hardware-impaired transmitter and receiver. The key idea of DDPM is to decompose the data generation process into subsequent “denoising” steps and then gradually generating the desired samples out of noise. Inspired by the recent visions on AI-native wireless for 6G [3]–[6], our general idea in this paper is that instead of designing a communication system which avoids hardware impairments (HWI) and estimation/decoding errors, we can train the network to handle such distortions. This way, the combined effect of hardware response and communication channel could be taken into account, introducing *native resilience* for wireless AI.

In our proposed scheme, a DDPM is employed at the receiver side (without relying on any other conventional autoencoder in contrast to [16]) to enhance the *resilience* of the wireless system against practical non-idealities such as HWIs, channel distortions, and quantization error. Our diffusion model-based receiver is parameterized by a neural network comprised of conditional linear layers (with softplus activation functions in hidden layers). In order to implement only one model for the entire denoising steps, the embeddings of time-steps are incorporated into each hidden layer of the model (more details are provided in the subsequent sections). The diffusion model is first trained to generate data samples out of noise. Then in the sampling (inference) phase, the reverse diffusion algorithm of DDPM is run at the receiver, starting from the batch of noisy and distorted received signals as input, until the original samples are reconstructed.

We show through extensive evaluations that our proposed approach can provide *native resilience* for communication systems in different scenarios, including low-SNR regimes, non-Gaussian noise, different HWI levels, and quantization error for both AWGN and fading scenarios. Our results show a *near-invariant* reconstruction performance with respect to channel noise and impairment levels, and *robust out-of-distribution performance* under non-Gaussian noise. Furthermore, we evaluate the reconstruction performance of our scheme in terms of cosine similarity and mean-squared error (MSE) metrics, highlighting more than 25 dB improvement in MSE compared to the conventional DNN-based receiver of [20], as one of the promising benchmark designs in ML-based communications systems for reconstruction tasks. Insightful data visualizations are also provided with respect to the training and sampling processes of the implemented diffusion model, by visualizing the output of the DDPM over time.

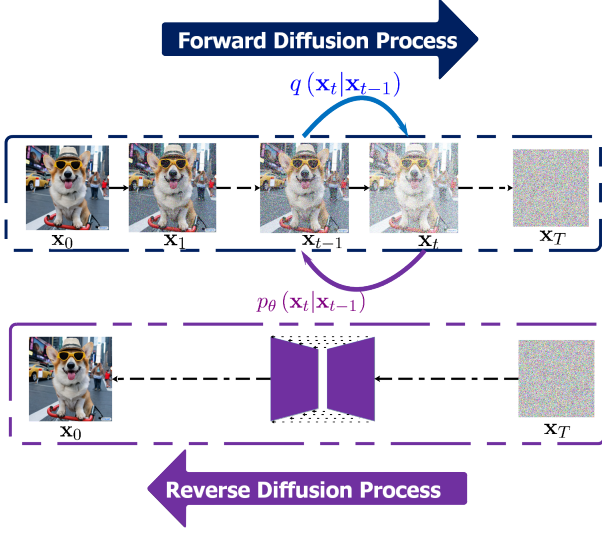


Fig. 1: Diffusion models: A general overview. A Markov chain is defined to mimic the forward diffusion steps, during which random perturbation noise is purposefully added to the original data. Then in a reverse process, the model learns to construct the desired data samples out of noise.

#### D. Paper Organization and Notations

The rest of the paper is organized as follows. In Section II, we first introduce the concept of DDPMs, the forward, and the reverse diffusion processes, together with the main formulas and the corresponding loss functions. We also try to point out insightful intuitions behind the main formulas of the DDPM framework. Our system model is introduced in Section III. We first provide the generic formulation of a communication system under non-linear HWIs. We then address the neural architecture and the algorithms used for training and sampling of our DDPM-based scheme. Numerical experiments are studied in Section IV. Finally, Section V concludes the paper.

*Notations:* Vectors and matrices are represented, respectively, by bold lower-case and upper-case symbols. Absolute value of a scalar variable and the  $\ell_2$  norm of a vector are denoted, respectively by  $|\cdot|$  and  $\|\cdot\|$ . Notation  $\mathcal{N}(\mathbf{x}; \boldsymbol{\mu}, \boldsymbol{\Sigma})$  stands for the multivariate normal distribution with mean vector  $\boldsymbol{\mu}$  and covariance matrix  $\boldsymbol{\Sigma}$  for a random vector  $\mathbf{x}$ . Similarly, complex normal distribution with the corresponding mean vector and covariance matrix is denoted by  $\mathcal{CN}(\boldsymbol{\mu}, \boldsymbol{\Sigma})$ . Moreover, the expected value of a random variable is denoted by  $\mathbb{E}[\cdot]$ . Sets are denoted by calligraphic symbols, and  $\mathbf{0}$  and  $\mathbf{I}$  show all-zero vector and identity matrix of the corresponding size, respectively. Moreover,  $[N]$ , (with  $N$  as integer) denotes the set of all integer values from 1 to  $N$ , and  $\text{Unif}[N]$ ,  $N > 1$ , denotes discrete uniform distribution with samples between 1 to  $N$ . Real and imaginary parts of a complex-valued vector are denoted by  $\Re\{\cdot\}$  and  $\Im\{\cdot\}$ , respectively.

## II. PRELIMINARIES ON DENOISING DIFFUSION PROBABILISTIC MODELS

Diffusion models are a new family of state-of-the-art probabilistic generative models which are inspired by non-equilibrium thermodynamics [18]. They are comprised of

two processes, namely the forward diffusion process and the parametric reverse diffusion process, as illustrated in Fig. 1. During the forward process, samples are diffused using Gaussian kernels to add noise until the fully-distorted signals follow an isotropic Gaussian distribution. Then in the reverse process, the model tries to “decode” the data via “denoising” the perturbed samples in a hierarchical fashion. Several diffusion-based generative models have been proposed in the ML literature with roughly similar underlying ideas. The models include diffusion probabilistic models [18], noise-conditioned score network (NCSN) [19], and denoising diffusion probabilistic models [7]. In this paper, we focus on DDPMs as the new state-of-the-art family of diffusion models. In what follows, we study the concept of DDPMs together with the main formulas and the corresponding loss functions. We also try to point out insightful intuitions behind the underlying formulas of the DDPM framework.

#### A. Forward Diffusion Process

Let  $\mathbf{x}_0$  be a data sample from some distribution  $q(\mathbf{x}_0)$ , i.e.,  $\mathbf{x}_0 \sim q(\mathbf{x}_0)$ . For a finite number,  $T$ , of time-steps, the forward diffusion process  $q(\mathbf{x}_t|\mathbf{x}_{t-1})$  is defined by adding Gaussian noise at each time-step  $t \in [T]$  according to a known “variance schedule”  $0 < \beta_1 < \beta_2 < \dots < \beta_T < 1$ . This can be formulated as

$$q(\mathbf{x}_t|\mathbf{x}_{t-1}) \sim \mathcal{N}(\mathbf{x}_t; \sqrt{1 - \beta_t}\mathbf{x}_{t-1}, \beta_t\mathbf{I}), \quad (1)$$

$$q(\mathbf{x}_{1:T}|\mathbf{x}_0) = \prod_{t=1}^T q(\mathbf{x}_t|\mathbf{x}_{t-1}). \quad (2)$$

Invoking (2), the data sample gradually loses its distinguishable features as the time-step goes on, where with  $T \rightarrow \infty$ ,  $\mathbf{x}_T$  approaches an isotropic Gaussian distribution with covariance matrix  $\boldsymbol{\Sigma} = \sigma^2\mathbf{I}$  for some  $\sigma > 0$  [7]. According to (1), each new sample at time-step  $t$  can be drawn from a conditional Gaussian distribution with mean vector  $\boldsymbol{\mu}_t = \sqrt{1 - \beta_t}\mathbf{x}_{t-1}$  and covariance matrix  $\boldsymbol{\Sigma}_t^2 = \beta_t\mathbf{I}$ . Hence, the forward process is realized by sampling from a Gaussian noise  $\boldsymbol{\epsilon}_{t-1} \sim \mathcal{N}(\mathbf{0}, \mathbf{I})$  and setting

$$\mathbf{x}_t = \sqrt{1 - \beta_t}\mathbf{x}_{t-1} + \sqrt{\beta_t}\boldsymbol{\epsilon}_{t-1}. \quad (3)$$

A useful property for the forward process in (3) is that we can sample  $\mathbf{x}_t$  at any arbitrary time-step  $t$  in a closed-form expression, through recursively applying the reparameterization trick from ML literature [21], and considering the sum properties of two Gaussian random variables. This results in the following formulation

$$\mathbf{x}_t = \sqrt{\bar{\alpha}_t}\mathbf{x}_0 + \sqrt{1 - \bar{\alpha}_t}\boldsymbol{\epsilon}_0, \quad (4)$$

$$q(\mathbf{x}_t|\mathbf{x}_0) \sim \mathcal{N}(\mathbf{x}_t; \sqrt{\bar{\alpha}_t}\mathbf{x}_0, (1 - \bar{\alpha}_t)\mathbf{I}), \quad (5)$$

where  $\bar{\alpha}_t = \prod_{i=1}^t (1 - \alpha_i)$  and  $\alpha_t = 1 - \beta_t$  [21]. Notably, (4) implies that one can directly sample  $\mathbf{x}_t$ ,  $t \in [T]$  from  $\mathbf{x}_0$ .

#### B. Parametric Reverse Diffusion Process

Now the problem is to reverse the process in (4) and sample from  $q(\mathbf{x}_{t-1}|\mathbf{x}_t)$ , so that we regenerate the true

samples from some Gaussian noise  $\mathbf{x}_T$ . According to [18], for  $\beta_t$  small enough,  $q(\mathbf{x}_{t-1}|\mathbf{x}_t), \forall t \in [T]$  also follows Gaussian distribution. However, we cannot easily estimate the distribution, since it requires knowing the distribution of all possible data samples (or equivalently exploiting the entire dataset) to be able to calculate the conditional probability. Hence, to approximate the conditional probabilities and run the reverse diffusion process, we need to learn a probabilistic model  $p_\theta(\mathbf{x}_{t-1}|\mathbf{x}_t)$  that is parameterized by  $\theta$ . According to the above explanations, the following expressions can be written

$$p_\theta(\mathbf{x}_{t-1}|\mathbf{x}_t) \sim \mathcal{N}(\mathbf{x}_{t-1}; \boldsymbol{\mu}_\theta(\mathbf{x}_t, t), \boldsymbol{\Sigma}_\theta(\mathbf{x}_t, t)), \quad (6)$$

$$p_\theta(\mathbf{x}_{0:T}) = p(\mathbf{x}_T) \prod_{t=1}^T p_\theta(\mathbf{x}_{t-1}|\mathbf{x}_t). \quad (7)$$

As can be seen from (6), the mean and variance of the reverse process are also conditioned on the time-step  $t$ . Now the problem simplifies to learning the mean vector  $\boldsymbol{\mu}_\theta(\mathbf{x}_t, t)$  and the covariance matrix  $\boldsymbol{\Sigma}_\theta(\mathbf{x}_t, t)$  for the probabilistic model  $p_\theta(\cdot)$ , where a neural network can be trained to approximate (learn) the reverse process with  $\theta$  showing the parameters of the neural network.

Before proceeding with the details of learning the reverse diffusion process, we note that if we condition the reverse process on  $\mathbf{x}_0$ , this conditional probability becomes tractable. The intuition behind this could be explained as follows. A painter (our generative model) requires a reference image  $\mathbf{x}_0$  to be able to gradually draw a picture. Hence, when we have  $\mathbf{x}_0$  as a reference, we can take a small step backwards from noise to generate the data samples, and the reverse step (drawing a picture in our metaphor) would be formulated as  $q(\mathbf{x}_{t-1}|\mathbf{x}_t, \mathbf{x}_0)$ . Mathematically speaking, by knowing the conditional probabilities of  $q(\mathbf{x}_t|\mathbf{x}_0)$  and  $q(\mathbf{x}_{t-1}|\mathbf{x}_0)$ , and utilizing Bayes rule, we can derive  $q(\mathbf{x}_{t-1}|\mathbf{x}_t, \mathbf{x}_0)$  with a similar expression to (6)

$$q(\mathbf{x}_{t-1}|\mathbf{x}_t, \mathbf{x}_0) \sim \mathcal{N}(\mathbf{x}_{t-1}; \tilde{\boldsymbol{\mu}}(\mathbf{x}_t, \mathbf{x}_0, t), \tilde{\beta}_t \mathbf{I}), \quad (8)$$

$$\tilde{\boldsymbol{\mu}}(\mathbf{x}_t, \mathbf{x}_0, t) = \frac{\sqrt{\alpha_t}(1 - \bar{\alpha}_{t-1})}{1 - \bar{\alpha}_t} \mathbf{x}_t + \frac{\sqrt{\bar{\alpha}_{t-1}}\beta_t}{1 - \bar{\alpha}_t} \mathbf{x}_0, \quad (9)$$

$$\tilde{\beta}_t = \frac{1 - \bar{\alpha}_{t-1}}{1 - \bar{\alpha}_t} \beta_t. \quad (10)$$

Invoking (8)–(10), one can infer that the covariance matrix in (8) has no learnable parameter. Hence, we simply need to learn the mean vector  $\tilde{\boldsymbol{\mu}}(\mathbf{x}_t, \mathbf{x}_0, t)$ . In the following, we first simplify (9), and then propose the DDPM-based training framework.

Thanks to the reparameterization trick and with a similar approach to (4), we can express  $\mathbf{x}_0$  as follows

$$\mathbf{x}_0 = \frac{1}{\sqrt{\bar{\alpha}_t}} (\mathbf{x}_t - \sqrt{1 - \bar{\alpha}_t} \boldsymbol{\epsilon}_t). \quad (11)$$

Substituting  $\mathbf{x}_0$  in (9) by (11) results in

$$\tilde{\boldsymbol{\mu}}(\mathbf{x}_t, \mathbf{x}_0, t) = \frac{1}{\sqrt{\alpha_t}} \left( \mathbf{x}_t - \frac{1 - \alpha_t}{\sqrt{1 - \bar{\alpha}_t}} \boldsymbol{\epsilon}_t \right). \quad (12)$$

Now we can learn the conditioned probability distribution  $p_\theta(\mathbf{x}_{t-1}|\mathbf{x}_t)$  of the reverse diffusion process by training a

neural network that approximates  $\tilde{\boldsymbol{\mu}}(\mathbf{x}_t, \mathbf{x}_0, t)$ . Therefore, we simply need to set the approximated mean vector  $\boldsymbol{\mu}_\theta(\mathbf{x}_t, t)$  to have the same form as the target mean vector  $\tilde{\boldsymbol{\mu}}(\mathbf{x}_t, \mathbf{x}_0, t)$ . Since  $\mathbf{x}_t$  is available at time-step  $t$ , we can reparameterize the neural network to make it approximate  $\boldsymbol{\epsilon}_t$  from the input  $\mathbf{x}_t$ . Compiling these facts results in the following expression for  $\boldsymbol{\mu}_\theta(\mathbf{x}_t, t)$

$$\boldsymbol{\mu}_\theta(\mathbf{x}_t, t) = \frac{1}{\sqrt{\alpha_t}} \left( \mathbf{x}_t - \frac{1 - \alpha_t}{\sqrt{1 - \bar{\alpha}_t}} \boldsymbol{\epsilon}_\theta(\mathbf{x}_t, t) \right), \quad (13)$$

where  $\boldsymbol{\epsilon}_\theta(\mathbf{x}_t, t)$  denotes our neural network.

We now define the loss function  $\mathcal{L}_t$  for time-step  $t$ , aiming to minimize the difference between  $\boldsymbol{\mu}_\theta(\mathbf{x}_t, t)$  and  $\tilde{\boldsymbol{\mu}}(\mathbf{x}_t, \mathbf{x}_0, t)$ .

$$\begin{aligned} \mathcal{L}_t &= \mathbb{E}_{\substack{t \sim \text{Unif}[T] \\ \mathbf{x}_0 \sim q(\mathbf{x}_0) \\ \boldsymbol{\epsilon}_0 \sim \mathcal{N}(0, \mathbf{I})}} \left[ \|\boldsymbol{\epsilon}_t - \boldsymbol{\epsilon}_\theta(\mathbf{x}_t, t)\|^2 \right] \\ &= \mathbb{E}_{\substack{t \sim \text{Unif}[T] \\ \mathbf{x}_0 \sim q(\mathbf{x}_0) \\ \boldsymbol{\epsilon}_0 \sim \mathcal{N}(0, \mathbf{I})}} \left[ \|\boldsymbol{\epsilon}_t - \boldsymbol{\epsilon}_\theta(\sqrt{\alpha_t} \mathbf{x}_0 + \sqrt{1 - \bar{\alpha}_t} \boldsymbol{\epsilon}_t, t)\|^2 \right]. \end{aligned} \quad (14)$$

Invoking (13) and (14), at each time-step  $t$ , the DDPM model takes  $\mathbf{x}_t$  as input and returns the distortion components  $\boldsymbol{\epsilon}_\theta(\mathbf{x}_t, t)$ . Moreover,  $\boldsymbol{\epsilon}_t$  denotes the diffused noise term at time-step  $t$ .

### III. SYSTEM MODEL AND PROPOSED SCHEME

In this section, we first present the system model under consideration and the corresponding formulations. We then address the neural architecture and the algorithms used for training and sampling of the employed DDPM.

#### A. Problem Formulation

Consider a point-to-point communication system with non-ideal hardware-impaired transceivers. Communication parties also carry out a finite-precision communication, in which data samples are first quantized, and then transmitted over the wireless channel. This is a practical assumption for resource-limited communication systems to strike a balance between reconstruction accuracy and communication efficiency.

We denote by  $s_k \in \mathbb{C}$ , the  $k$ -th element,  $k \in [K]$ , in the batch (with size  $K$ ) of unit-power data samples that are supposed to be sent over the channel. Also, we denote by  $s_k^q$ , the quantized version of  $s_k$ . This can be modeled by  $s_k^q = s_k + e_k^q$  with  $e_k^q$  denoting the quantization error due to finite precision mapping from the continuous-valued signals to a discrete space. Wireless channel between the communication entities follows block-fading model, and is represented by a complex-valued scalar  $h_k \in \mathbb{C}, \forall k \in [K]$ , taking independent realizations within each coherence block. Accordingly, the received signal  $y_k$  under HWIs and finite-precision transmission is formulated by<sup>3</sup>

$$y_k = h_k(\sqrt{p}s_k^q + \eta_k^t) + \eta_k^r + n_k, \quad (15)$$

$$\eta_k^t \sim \mathcal{CN}(0, \kappa^t p), \quad \eta_k^r \sim \mathcal{CN}(0, \kappa^r p |h_k|^2), \quad (16)$$

<sup>3</sup>To make our formulations more tractable, we consider the single-antenna notations. Nevertheless, our approach is generic, and it is applicable to the multi-antenna scenario, as will be shown in Section IV.

where  $p$  denotes the transmit power,  $\eta_k^t$  is the distortion noise caused by the transmitter hardware with the corresponding impairment level  $\kappa^t$ . Moreover,  $\eta_k^r$  reflects the hardware distortion at the receiver with  $\kappa^r$  showing the level of impairment at the receiver hardware. Notably,  $\eta_k^r$  is conditionally Gaussian, given the channel realization  $h_k$ . This is a well-known and experimentally-validated model for HIs, which is widely-adopted in wireless communication literature [23]. To further explain (15), we emphasize that according to [23], the distortion noise caused at each radio frequency (RF) device is proportional to its signal power. Notably, in addition to the receiver noise  $n_k$  that models random fluctuations in the electronic circuits of the receiver, a fixed portion of the information signal is turned into *distortion noise* due to quantization errors in analog-to-digital converter (ADC), inter-carrier interference induced by phase noise, leakage from the mirror subcarrier under I/Q imbalance, nonlinearities in power amplifiers, etc. [23].

*Remark 1:* The power of distortion noise is proportional to the signal power  $p$  and the channel gain  $|h_k|^2$ . According to [23], HWI levels,  $\kappa^t$  and  $\kappa^r$ , characterize the proportionality coefficients and are related to the error vector magnitude (EVM). Following [23], we consider  $\kappa$ -parameters in the range  $[0, 0.15^2]$  in our simulations, where smaller values imply less-impaired transceiver hardware.

To be aligned with the “batch-processing” nature of AI/ML algorithms and wireless communications simulators [22], we formulate our signaling expressions in matrix-based format. To do so, we define the batch of data samples as  $\mathbf{s} \triangleq [s_1, s_2, \dots, s_K]^T$  with the underlying distribution  $\mathbf{s} \sim q(\mathbf{s})$ . Hence, the received batch  $\mathbf{y} \in \mathbb{C}^K$  of noisy-and-distorted signals at the receiver can be expressed as

$$\mathbf{y} = \sqrt{p} \mathbf{H} \mathbf{s} + \boldsymbol{\zeta}, \quad (17)$$

where  $\mathbf{H} = \text{diag}(\mathbf{h})$  and  $\mathbf{h} \triangleq [h_1, h_2, \dots, h_K]^T$  stands for the corresponding channel realizations vector corresponding to the transmission of batch samples. Moreover,  $\boldsymbol{\zeta} \triangleq \mathbf{H}(\boldsymbol{\eta}^t + \sqrt{p} \mathbf{e}^q) + \boldsymbol{\eta}^r + \mathbf{n}$  represents the effective Gaussian noise-plus-distortion at the receiver with the conditional distribution  $\boldsymbol{\zeta} | \mathbf{h} \sim \mathcal{CN}(\mathbf{0}_K, \boldsymbol{\Sigma})$  and the covariance matrix  $\boldsymbol{\Sigma}$  given by  $\boldsymbol{\Sigma} = p(\kappa^t + \kappa^r) \mathbf{G} + \sigma^2 \mathbf{I}_K$ . We also define

$$\boldsymbol{\eta}^t \triangleq [\eta_1^t, \eta_2^t, \dots, \eta_K^t]^T \sim \mathcal{CN}(\mathbf{0}_K, \kappa^t p \mathbf{I}_K), \quad (18)$$

and

$$\boldsymbol{\eta}^r \triangleq [\eta_1^r, \eta_2^r, \dots, \eta_K^r]^T \sim \mathcal{CN}(\mathbf{0}_K, \kappa^r p \mathbf{G}), \quad (19)$$

which is conditionally Gaussian given the channel realizations  $\{h_k\}_{k \in [K]}$ , with  $\mathbf{G} = \text{diag}([|h_1|^2, |h_2|^2, \dots, |h_K|^2]^T)$ . We also have  $\mathbf{e}^q \triangleq [e_1^q, e_2^q, \dots, e_K^q]^T$  and  $\mathbf{n} \sim \mathcal{CN}(\mathbf{0}_K, \sigma^2 \mathbf{I}_K)$ .

Due to the fact that neural networks can only process real-valued inputs, we map complex-valued symbols to real-valued tensors, and rewrite (17) by stacking the real and imaginary components. This results in the following expression.

$$\mathbf{y}_r = \tilde{\mathbf{H}} \mathbf{x} + \boldsymbol{\nu}, \quad (20)$$

where

$$\mathbf{y}_r = \begin{bmatrix} \Re\{\mathbf{y}\} \\ \Im\{\mathbf{y}\} \end{bmatrix} \in \mathbb{R}^{2K}, \quad (21)$$

$$\mathbf{x} = \sqrt{p} \begin{bmatrix} \Re\{\mathbf{s}\} \\ \Im\{\mathbf{s}\} \end{bmatrix} \in \mathbb{R}^{2K}, \quad (22)$$

$$\tilde{\mathbf{H}} = \begin{bmatrix} \Re\{\mathbf{H}\} & -\Im\{\mathbf{H}\} \\ \Im\{\mathbf{H}\} & \Re\{\mathbf{H}\} \end{bmatrix} \in \mathbb{R}^{2K \times 2K}, \quad (23)$$

$$\boldsymbol{\nu} = \begin{bmatrix} \Re\{\boldsymbol{\zeta}\} \\ \Im\{\boldsymbol{\zeta}\} \end{bmatrix} \in \mathbb{R}^{2K}. \quad (24)$$

*Remark 2:* For the completeness of our formulations, we also note that the covariance matrix of  $\boldsymbol{\nu}$  could be formulated as

$$\mathbf{C} = \frac{1}{2} \begin{bmatrix} \Re\{\boldsymbol{\Sigma}\} & -\Im\{\boldsymbol{\Sigma}\} \\ \Im\{\boldsymbol{\Sigma}\} & \Re\{\boldsymbol{\Sigma}\} \end{bmatrix} \in \mathbb{R}^{2K \times 2K}. \quad (25)$$

This can be obtained due to the fact that the effective noise-plus-distortion term  $\boldsymbol{\zeta}$  in (24) is conditionally circularly symmetric given the channel realizations vector.

### B. Proposed Solution: Algorithms & Neural Network Architecture

In this subsection, we propose the DDPM framework for the communication system formulated in Section III-A. Within our diffusion-based communication scheme, a DDPM is first trained with the objective of regenerating the diffused ground-truth samples out of the noise. Afterward, the DDPM-based framework can be run in the communication system to remove the impairments and distortions from the batch of distorted received signals, i.e.,  $\mathbf{y}_r$  in (20). This way, the combined effect of hardware and channel distortions and residual errors is taken into account by leveraging the “denois-and-generation” capability of diffusion models. The performance of this generative AI-based communication system is then verified in the next section, highlighting *network resilience* for a generic wireless system with practical non-idealities of HWIs and quantized data transmission.

1) *Training and Sampling Algorithms:* In brief, the idea here is to first make our system learn how to gradually remove the random noise from batches of purely noisy samples  $\mathbf{x}_T$ . This is done via exploiting the realizations of the original distribution  $q(\cdot)$ , or equivalently the training samples of a dataset with the corresponding empirical distribution  $q(\cdot)$ . Then in the inference phase, which is called sampling in the ML literature, we start from the distorted batch of received signals in (20), run the DDPM framework to remove the hardware and channel distortions and residual errors, and reconstruct original samples  $\mathbf{x} \sim q(\mathbf{x})$ . During the training phase, both forward and reverse diffusion processes are run, while the sampling phase corresponds to the reverse diffusion process.

Our diffusion model is trained based on the loss function given in (14), which calculates the MSE between the true and the predicted distortion noise. In (14),  $\mathbf{x}_0$  can be interpreted as a data sample from a training set with unknown and possibly complicated underlying distribution  $q(\cdot)$ . Moreover,  $\epsilon_t$  denotes the diffused noise term sampled at time-step  $t$ ,

---

**Algorithm 1** Training algorithm of DDPM
 

---

**Hyper-parameters:** Number of time-steps  $T$ , neural architecture  $\epsilon_\theta(\cdot, t)$ , variance schedule  $\beta_t$ , and  $\bar{\alpha}_t, \forall t \in [T]$ .

**Input:** Training samples  $\mathbf{x}_0 \sim q(\mathbf{x}_0)$  from a dataset  $\mathcal{S}$ .

**Output:** Trained neural model for DDPM.

- 1: **while** the stopping criteria are not met **do**
  - 2:   Randomly sample  $\mathbf{x}_0$  from  $\mathcal{S}$
  - 3:   Randomly sample  $t$  from  $\text{Unif}[T]$
  - 4:   Randomly sample  $\epsilon$  from  $\mathcal{N}(\mathbf{0}_{2K}, \mathbf{I}_{2K})$
  - 5:   Take gradient descent step on
  - 6:      $\nabla_\theta \|\epsilon - \epsilon_\theta(\sqrt{\bar{\alpha}_t}\mathbf{x}_0 + \sqrt{1 - \bar{\alpha}_t}\epsilon, t)\|^2$
  - 7: **end while**
- 

and  $\epsilon_\theta(\mathbf{x}_t, t)$  denotes the approximated noise-plus-distortion at the output of the neural network. According to the loss function in (14), we note that  $\bar{\alpha}_t, \forall t \in [T]$ , is a function of the variance scheduling  $\beta_t$  that we design. In other words,  $\bar{\alpha}_t$ 's are known and can be designed beforehand. This means that by properly designing the variance scheduling for our forward diffusion process, we can optimize a wide range of desired loss functions  $\mathcal{L}_t$  during training. Equivalently, one can randomly sample  $t \in [T]$  and optimize the corresponding loss function, so that, intuitively, the neural network would be able to “see” different structures of the distortion noise during its training, making it robust against a wide range of distortion levels when sampling.

The training process is summarized in Algorithm 1. We take a random sample  $\mathbf{x}_0$  from the raining set  $\mathcal{S}$ . We also sample a random time-step  $t \sim \text{Unif}[T]$  to be encoded as time embedding for our conditional neural layers. A noise vector  $\epsilon$  (with the same shape as the input) is also sampled from normal distribution, and the input is distorted by this noise. The desired noise level is adjusted according to the designed “variance scheduling”  $\beta_t$ . Then the neural network is trained to estimate the noise vector in the distorted data, using the loss function given in (14). The network is optimized using stochastic gradient descent algorithms on the batches of data samples. It takes the noisy samples and the time embeddings as input, and returns the approximated noise vector as output. Fig. 2 illustrates this process.

We now elaborate on the sampling phase which corresponds to the reverse diffusion process. The sampling method is summarized in Algorithm 2. We start from the received batch of distorted signals  $\mathbf{y}_r$ , and then iteratively denoise it using the trained neural network  $\epsilon_\theta(\mathbf{x}_t, t)$  at each time-step until we end up at  $t = 0$ . More specifically, starting from  $\mathbf{y}_r$ , for each time-step  $t \in \{T, T-1, \dots, 1\}$ , the neural network outputs  $\epsilon_\theta(\mathbf{x}_t, t)$  to approximate the residual noise-plus-distortion within the batch of received signals. A sampling algorithm is then run as expressed in step 4 of Algorithm 2, in order to sample  $\mathbf{x}_{t-1}$ . The process is executed for  $T$  time-steps until  $\mathbf{x}_0$  is reconstructed ultimately.

2) *Neural Network Architecture:* Generally speaking, the implemented neural network should take as input the tensor of noisy signals at a particular time-step, and approximate distortions-plus-noise as the output, as elaborated in Algorithm 1. The approximated distortions-plus-noise vector

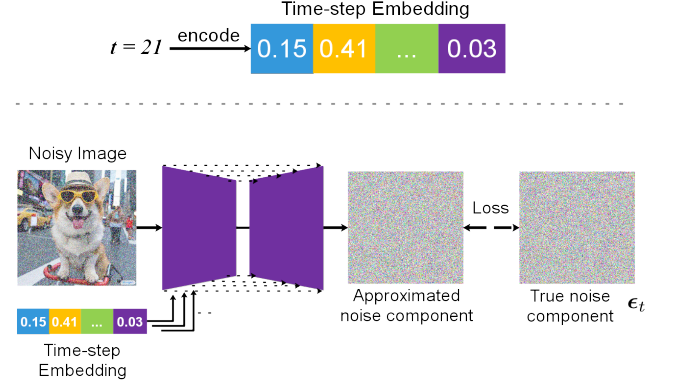


Fig. 2: General description of training the diffusion model.

---

**Algorithm 2** Sampling algorithm of DDPM
 

---

- 1:  $\mathbf{x}_T = \mathbf{y}_r$
  - 2: **for**  $t = T, \dots, 1$  **do**
  - 3:    $\mathbf{z} \sim \mathcal{N}(\mathbf{0}_{2K}, \mathbf{I}_{2K})$  if  $t > 1$ , else  $\mathbf{z} = \mathbf{0}_{2K}$
  - 4:    $\mathbf{x}_{t-1} = \frac{1}{\sqrt{\alpha_t}} \left( \mathbf{x}_t - \frac{1-\alpha_t}{\sqrt{1-\alpha_t}} \epsilon_\theta(\mathbf{x}_t, t) \right) + \sqrt{1-\alpha_t} \mathbf{z}$
  - 5: **end for**
  - 6: **return**  $\mathbf{x}_0$
- 

would be a tensor with the same size as the input tensor. Therefore, the neural network should output tensors of the same shape as its input at every time-step  $t \in T$ . Instead of training  $T$  distinct models for each time-step, the hidden layers of the neural network can be conditioned on  $t$ . Intuitively, this makes the model “know” at which particular time-step it is operating for every sample in the batch. We also remark that the notion of time-step equivalently corresponds to the level of residual noise-plus-distortion in the batch of received signals. This is verified in our simulation results in Section IV, where data samples with different levels of “noisiness” can be observed at different time-steps  $t \in [T]$ .

Based on the above-mentioned explanations, our DDPM is parameterized by a neural network  $\epsilon_\theta(\cdot, t)$  with 3 conditional hidden layers, each of which has 128 neurons with Softplus activation functions. The output layer is a simple linear layer with the same size as the input. To enable employing only one neural network for the entire denoising steps, we share the parameters of the neural network across time-steps. More specifically, as shown in Fig. 2, we encode the time-steps  $t \in [T]$  and input it to each hidden layer of our neural network as a vector embedding. The hidden layers are conditioned on  $t$  via being multiplied by the time embeddings [7], [9], [12]. Training of this model can be carried out at the edge server (employed e.g., at the base station of 6G network) or at the central cloud server, and then downloaded by the receiver end for the inference phase.

#### IV. NUMERICAL RESULTS

In this section, we provide different numerical evaluations to highlight the performance of our proposed approach



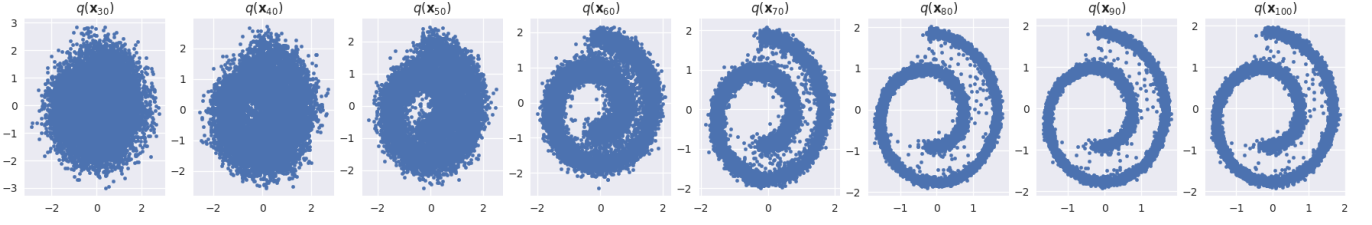


Fig. 3: Data visualization for the reverse diffusion process over different time steps during the training of our diffusion model. From left to right, the output of the DDPM is visualized over time-steps  $t = \{30, 40, \dots, 100\}$  while being trained.

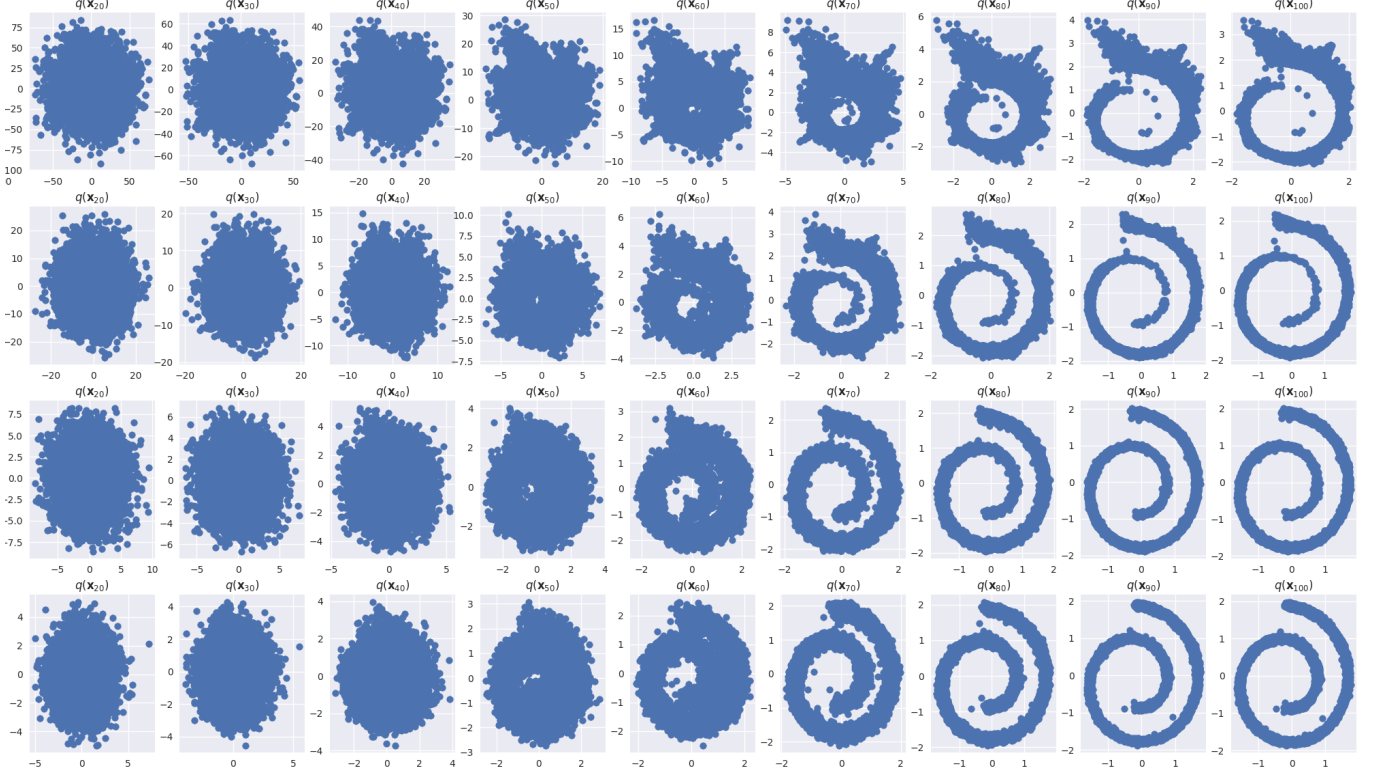


Fig. 4: Data visualization of the denoising process during sampling phase. From top to bottom, the rows respectively correspond to SNR values  $\Gamma = \{-30, -20, -10, 0\}$  dB over Rayleigh fading communication channel.

in different scenarios and compared to different baselines. We also evaluate the *resilience* of our proposed scheme in different scenarios. Specifically, we demonstrate remarkable reconstruction performance in low-SNR regimes, as well as robust OOD performance under non-Gaussian assumption. In addition, the system shows resilient near-“invariant” performance across a wide range of hardware impairment levels and quantization resolutions. We also evaluate the reconstruction performance of our DDPM-based scheme compared to the conventional DNN-based receiver proposed in [20] as one of the seminal benchmarks for ML-based communications systems.

As discussed in Section III-B, our employed neural network is comprised of 3 conditional hidden linear layers, each of which has 128 neurons with softplus activation functions. The output layer is a simple linear layer with the same shape as input. We employ one neural network for the entire time-steps. To do so, we encode the time-step  $t$ , and incorporate it into each hidden layer of our neural network

as an input embedding. To stabilize the training algorithm of the DDPM framework, exponential moving average (EMA) method is implemented. This helps maintain a form of “model momentum.” Specifically, instead of directly updating model’s weights, a copy of the previous weights is kept, and the weighted average between the previous and new version of the weights are calculated for the model update [24]. For the diffusion process, we set  $T = 100$  time-steps, and the variance schedule  $\alpha_t$  is set to constants decreasing from  $\alpha_1 = 0.99999$  to  $\alpha_T = 0.99$  with Sigmoid scheduling. For optimizing the neural network hyperparameters, we use adaptive moment estimation (Adam) optimizer with learning rate  $\lambda = 10^{-3}$  over 2000 epochs. That is, similar to [11]–[13], [16], the stopping criterion in Algorithm 1 is set to reaching the maximum number of epochs. In this section, transmit SNR is defined as

$$\Gamma = 10 \log_{10} \left( \frac{p}{\sigma^2} \right) \text{ dB}. \quad (26)$$

Without loss of generality, we set the average signal power to

$p = 1$  for all experiments, while varying the SNR by setting the standard deviation (std) of noise  $\sigma$  [27].

#### A. Data Visualization for Training and Sampling Processes

In this subsection, the denoising and generation performance of the diffusion model during training and sampling phases are visualized over swiss roll dataset with 10000 samples [18], [25]. For the following figures, we set  $\kappa^t = 0.05$  and  $\kappa^r = 0.15$  [23], unless otherwise stated. The effect of different impairment levels is studied in the next subsection.

Fig. 3 visualizes the reverse diffusion process over different time-steps during the training of our diffusion model. Specifically, the output of the DDPM in different time-steps is visualized while being trained. This could be done thanks to the fact that we share the parameters of the model across time-steps via incorporating the time-step embeddings into the hidden layers of our neural network. Hence, it is known that at which particular time-step the model is operating, and we visualize it. As can be seen from the figure, our DDPM gradually learns to denoise and generate samples out of an isotropic Gaussian distribution. The figure also highlights the fact that the notion of time-step equivalently corresponds to the level of residual noise in the batch of signals, where data samples with different levels of “noisiness” can be observed at different time-steps  $t \in [T]$  from left to right. This verifies our claims in Section III-B.

In Fig. 4, we present our data visualization for the sampling phase. For this figure, we run the trained DDPM and took “snapshots” at specific time-steps (every 10 steps). This is repeated for different SNRs to visualize denoising-and-generation performance of our DDPM under different levels of noise. According to the figure, even when the power of noise is more than 300 times of the signal, i.e.,  $\Gamma = -25$ , we can have a clear understanding of the underlying distribution, while having  $\Gamma = -15$  dB is enough to clearly reconstruct data samples. Moreover, we can infer from the figure that for heavily-distorted scenarios such as  $\Gamma = -30$  dB or  $\Gamma = -25$  dB, the diffusion model is able to learn the data points corresponding to outer part of the distribution. Intuitively, this shows that the model has smartly decided to focus on the easier (less complicated) parts of data distribution, and ignore the tricky part of the internal semicircle to have as little reconstruction error as possible. This is quantitatively studied in the next subsection.

#### B. Reconstruction Performance in Different Scenarios

In this subsection, we study the reconstruction performance of our proposed scheme in low-SNR regimes, non-Gaussian noise, HWI distortion, and quantization errors. We consider AWGN channel for Fig. 5, (we also study the effect of non-Gaussian additive noise in this figure), while for the rest of the figures, complex-valued Rayleigh fading channels are considered. For Figs. 5, 6, 7, and 11, we set  $\kappa^t = 0.05$  and  $\kappa^r = 0.15$  [23], while we study the effect of different impairment levels in Figs. 8, 9, and 10. The effect of the number of quantization bits on our DDPM-based finite-precision communication is studied in Figs. 6, 7, and 11. For

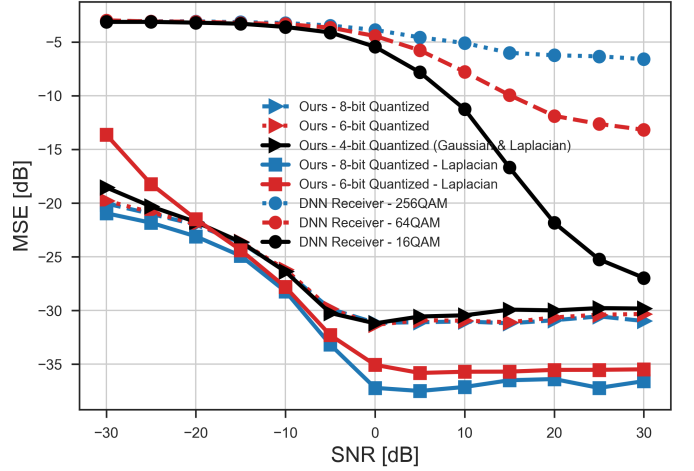


Fig. 5: MSE between the original signal and the reconstructed one under AWGN channel and non-Gaussian additive noise for our scheme and [20] as benchmark.

the rest of the figures, data samples are represented by 8 bits before being transmitted over the wireless channel.

Fig. 5 demonstrates the reconstruction performance of our DDPM-based scheme compared to the conventional DNN-based benchmark [20] over a wide range of SNR values  $-30 \text{ dB} \leq \Gamma \leq 30 \text{ dB}$ . In this experiment, the MSE metric (averaged over 10 runs of sampling) between the original and reconstructed data samples is considered for evaluation. Since we have employed our diffusion model at the receiver end, we only exploit the receiver DNN of [20], and fine-tune it for benchmarking, so that we can have a fair comparison. For the DNN, three hidden linear layers with 64 neurons and rectified linear unit (ReLU) activation functions are considered. Based on our ablation studies, increasing the depth of the conventional DNN, or the number of hidden neurons does not result in any significant improvement in its performance. For this experiment, the original data samples are first quantized into bitstreams, and then mapped to QAM symbols (as a widely-adopted constellation format in wireless networks [3], [4]) to be transmitted over the wireless channel. For 16- and 64-QAM scenarios, we considered 5000 training iterations, while for 256-QAM, the DNN was trained for 30000 iterations with Adam optimizer and learning rate  $\lambda = 0.01$  [22]. Notably, Fig. 5 highlights significant improvement in reconstruction performance among different quantization resolutions and across a wide range of SNR values, specially in low-SNR regimes. For instance, considering 0 dB SNR and 64-QAM scenario, more than 25 dB improvement is achieved via our DDPM compared to the the well-known model of [20], which is a widely-adopted benchmark for ML-based communications systems. Fig. 5 also highlights the *resilience* of our approach against non-Gaussian noise. For this benchmark, we consider additive Laplacian noise with the same variance as that of AWGN scenario [3]. Remarkably, although we do not re-train our diffusion model under Laplacian noise, the performance of our DDPM-based approach does not change (or even becomes better in some cases) under this non-Gaussian assumption.



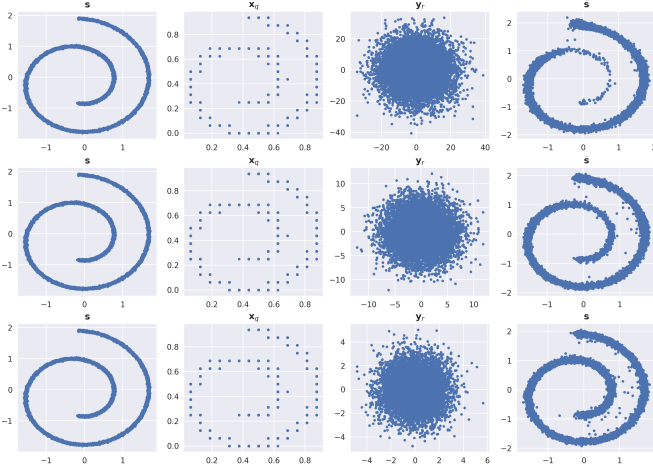


Fig. 6: Reconstruction performance of DDPM in finite-precision communications with 4 bits quantization. From left to right, the original samples, the quantized version sent over the wireless channel, the received data and the reconstructed data are illustrated. The rows correspond to SNR values  $\Gamma = \{-20, -10, 0\}$  dB, respectively.

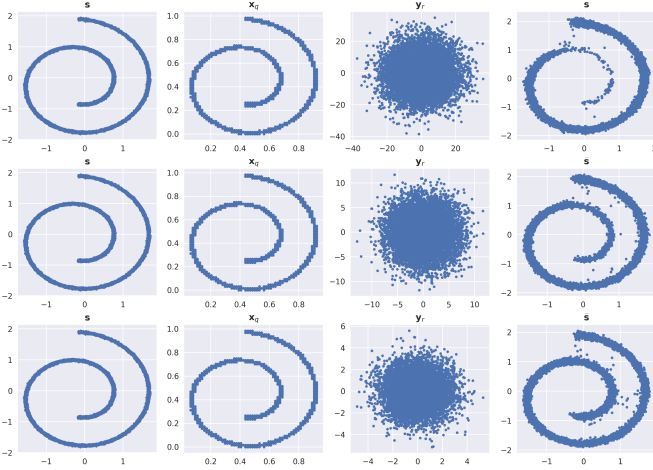


Fig. 7: Reconstruction performance of DDPM in finite-precision communications with 6 bits quantization. From left to right, the original samples, the quantized version sent over the wireless channel, the received signal, and the reconstructed data are illustrated. The rows correspond to SNR values  $\Gamma = \{-20, -10, 0\}$  dB, respectively.

However, we can see from the figure that the DNN-based benchmark experiences significant performance degradation under non-Gaussian assumption, although we also re-trained it with Laplacian additive noise instead of AWGN channel. This clearly highlights the *robust OOD performance* of our proposed scheme.

Figs. 6 and 7 demonstrate the reconstruction performance of the DDPM in finite-precision communications, when data samples are represented by 4 and 6 bits, respectively. Both of the figures clearly highlight the performance of the employed diffusion-based scheme in removing the negative effects of representing signals with finite precision, and also the channel distortion and receiver noise. Notably, even when the continuous-valued signals are represented in a low resolution

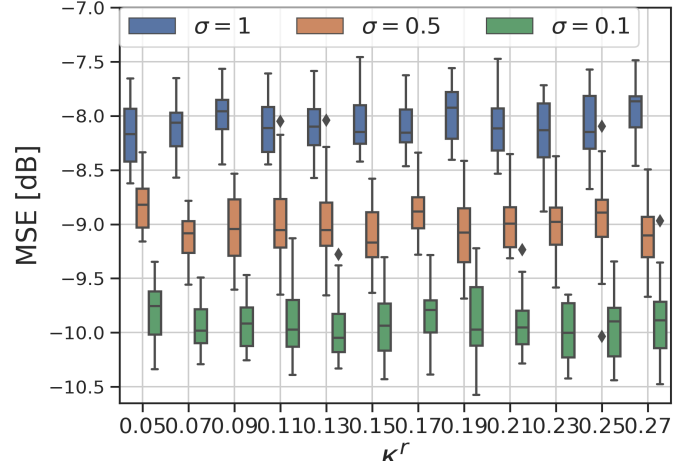


Fig. 8: MSE between the original signal and the reconstructed one for different levels of hardware impairment.

format, (e.g., 4 bits as shown in Fig. 6), the trained DDPM shows a notable performance in regenerating the original samples out of heavily-distorted signals  $y_r$ , for a wide range of low-SNR values between  $-20$  dB to  $5$  dB.

Fig. 8 studies the effect of different HWI levels on the reconstruction performance of our scheme over Rayleigh fading channels. For this figure, we set  $\kappa^t = 0.05$  and vary the impairment level of the receiver,  $\kappa^r$ , over the typical ranges specified in Ref. [23]. The reconstruction results are obtained in terms of MSE metric over 20 realizations of the system. The figure highlights an important characteristic of our proposed scheme. Our DDPM-based communication system is *resilient* against hardware distortions, since the reconstruction performance does not change with the increase in the impairment level. Notably, our DDPM-based scheme showcases a *near-invariant* reconstruction performance with respect to noise and impairment levels, which also highlights the generalizability of the proposed approach. This is achieved due to the so-called “variance scheduling” of our DDPM framework in (3), which allows the system to become robust against a wide range of distortions caused by channel and hardware impairments.

In Figs. 9 and 10, we study the reconstruction quality of our scheme in terms of two other measures, i.e., the normalized MSE (NMSE) [12], and the cosine similarity [28] between the original data and the reconstructed version, for both scenarios of single-antenna and multi-antenna transmission (with 4 transmitting antennas). The NMSE is defined as

$$\text{NMSE [dB]} = 10 \log_{10} \frac{\|\mathbf{x} - \hat{\mathbf{x}}\|^2}{\|\mathbf{x}\|^2}. \quad (27)$$

Moreover, the cosine similarity is a widely-adopted measure in data science to quantify the similarity between two vectors,  $\mathbf{x}$  and  $\hat{\mathbf{x}}$ . It can be formulated as given below

$$\text{CSIM} = \frac{\mathbf{x}^\top \hat{\mathbf{x}}}{\|\mathbf{x}\| \|\hat{\mathbf{x}}\|}. \quad (28)$$

The figure highlights that even for very low SNR regimes, e.g.,  $\Gamma = -30$  dB, the reconstructed signals maintain

the underlying similarity to the original data, as can be seen from the corresponding values of NMSE and cosine similarity in the figure. Moreover, increasing the transmit SNR, the reconstruction performance significantly improves. This numerically verifies our data visualization results and discussions provided for Fig. 4. Our results in Figs. 9 and 10 also verify the *resilience* of our scheme under different HWI levels. Notably, although it is shown in [26] that having imbalanced HWIs at transceiver chains (i.e.,  $\kappa^t \neq \kappa^r$ ) could result in more performance degradation in conventional wireless systems, our DDPM-based scheme shows resilience against such imbalanced scheme, as the NMSE and cosine similarity metrics are almost similar in both cases of  $(\kappa^t, \kappa^r) = (0.05, 0.15)$  and  $(\kappa^t, \kappa^r) = (0.10, 0.10)$ . To show the generalizability of our proposed approach, we further apply our solution to multi-antenna (MA) setup, in both cases of having the CSI knowledge at the transmitter (with CSIT) or not (without CSIT). According to the figure, it is interesting to see that when the transmitter does not have the CSI knowledge, the reconstruction performance drops compared to the single-antenna case. This is due to the fact that in a communication system with practical hardware impairments, having more hardware-impaired transmitting antennas results in the increased aggregation of distortion noise. Hence, the accumulation of these impairments can degrade the reconstruction performance of the receiver to some extent. Moreover, the saturation in high SNR values is due to the fact that the HWI distortion is also intensified with the increase in power  $p$  as discussed in Remark 1. This also verifies our communication framework proposed in Section III-A. Still, original data samples can be reconstructed well with  $\text{NMSE} = 0.00025$  and cosine similarity of almost 0.99. On the other hand, when we have the CSI knowledge at transmitter, employing multiple antennas can help compensate for the fading effects of wireless channel, which can make it easier for the receiver DDPM to focus on removing hardware distortions (than channel distortions), resulting in a better performance. Accordingly, our results show that almost lossless decoding is achieved with near-zero NMSE, when having transmit SNRs of  $\Gamma \geq 10$  dB.

Fig. 11 demonstrates the reconstruction performance of our scheme, in terms of cosine similarity (averaged over 20 runs of sampling algorithm), with respect to different resolutions in representing data samples. For this experiment, the cosine similarity between the vector of original data samples (before quantization) and the reconstructed ones is calculated for different quantization resolutions. This figure numerically verifies our results illustrated in Figs. 6 and 7. Remarkably, the figure highlights that having the quantized versions sent over the wireless channels, still we can reconstruct data samples with almost perfect similarity ( $\text{CSIM} > 0.99$ ) to the original input. We can also infer from the figure that a near-invariant reconstruction performance is achieved with respect to different precision levels, as the cosine similarity values follow the same trend in all of the three scenarios. This could be a motivation for future research on diffusion-based communication schemes, in terms of maintaining a balance between energy efficiency and reconstruction accuracy over

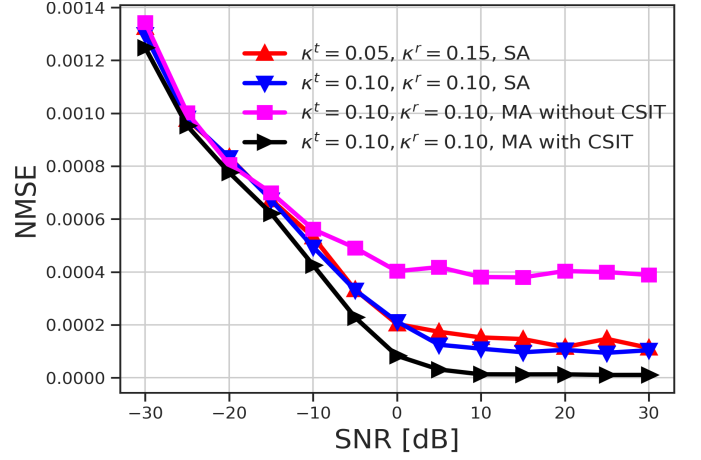


Fig. 9: NMSE vs. SNR for our scheme in single-antenna and multi-antenna scenarios with 4 transmitting antennas.

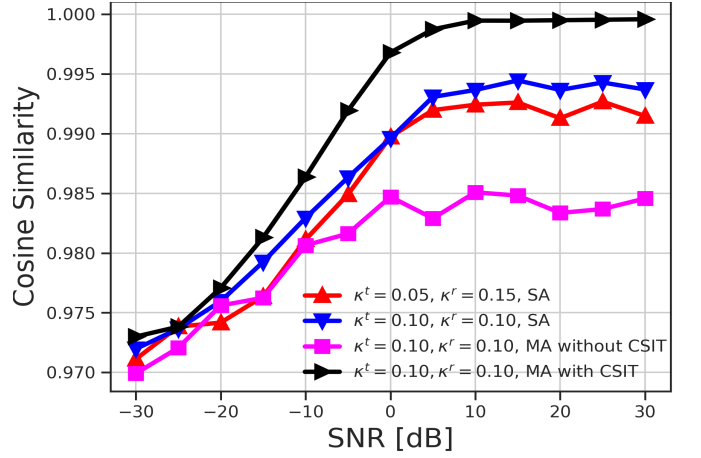


Fig. 10: Cosine similarity vs. SNR for our scheme in single-antenna and multi-antenna scenarios with 4 transmitting antennas.

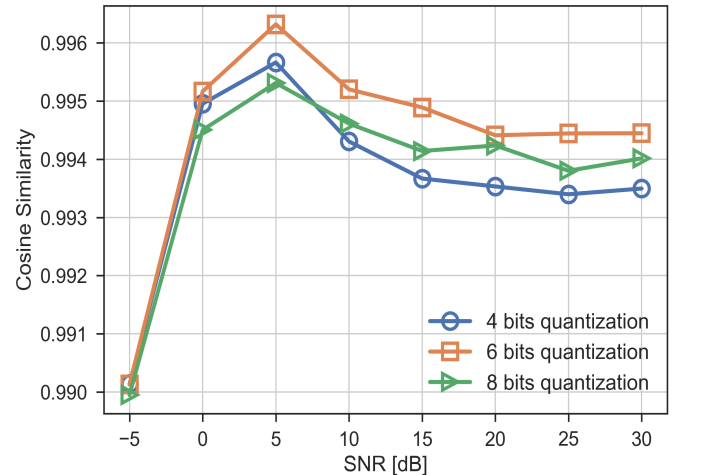


Fig. 11: Effect of quantization on the reconstruction performance in terms of cosine similarity.

wireless networks with limited available radio resources.

## V. CONCLUSIONS AND FUTURE WORKS

In this paper, we have proposed DDPMs for finite-precision wireless communication system with hardware-impaired transceivers. First, we have introduced the key concepts of diffusion modeling, together with the intuitions behind the DDPM framework. Next, our proposed scheme has been introduced via providing the generic formulations, the neural architecture, and the training and sampling algorithms of our DDPM-based scheme. Through extensive numerical experiments, we have evaluated the reconstruction performance of our scheme in terms of cosine similarity and MSE, highlighting more than 25 dB improvement compared to the conventional DNN-based approach. We have shown that our proposed approach provides native resilience for communication systems under low-SNR regimes, as well as near-invariant reconstruction performance with respect to different HWI levels and quantization resolutions. Furthermore, a robust OOD performance under non-Gaussian noise has been shown for the proposed scheme.

Thanks to the outstanding capabilities of diffusion models to learn the patterns and generate “highly-structured” data samples, DDPMs can also be employed for emerging technologies at the intersection of 6G networks and Metaverse systems. One of the main challenges for realizing such systems lies within data privacy concerns [27], [29]–[31], as well as the hallucination effects exhibited by generative models in generative AI paradigm. We will investigate such systems in our future works.

## REFERENCES

- [1] M. Letafati, S. Ali, M. Latva-aho, “Denoising diffusion probabilistic models for hardware-impaired communications,” *arXiv preprint arXiv:2309.08568*, Oct. 2023.
- [2] M. Letafati, S. Ali, and M. Latva-aho, “WiGenAI: The symphony of wireless and generative AI via diffusion models,” *arXiv preprint arXiv:2310.07312*, Oct. 2023.
- [3] M. Chafii, L. Bariah, S. Muhaidat, and M. Debbah, “Twelve scientific challenges for 6G: Rethinking the foundations of communications theory,” *IEEE Communications Surveys & Tutorials*, vol. 25, no. 2, pp. 868–904, Second quarter 2023.
- [4] M. Merluzzi et al., “The Hexa-X project vision on artificial intelligence and machine learning-driven communication and computation co-design for 6G,” *IEEE Access*, vol. 11, pp. 65620–65648, Jun. 2023.
- [5] 3GPP Release 18, “Study on Artificial Intelligence (AI)/Machine Learning (ML) for NR Air Interface RAN,” Meeting #112, Athens, Greece, Tech. Rep., 27th February – 3rd March 2023.
- [6] S. Ali, et al., “6G white paper on machine learning in wireless communication networks,” *arXiv preprint arXiv:2004.13875*, 2020.
- [7] J. Ho, A. Jain, and P. Abbeel, “Denoising diffusion probabilistic models,” *Advances in Neural Information Processing Systems*, vol. 33, pp. 6840–6851, 2020.
- [8] B. Levac, A. Jalal, K. Ramchandran, and J. I. Tamir, “MRI reconstruction with side information using diffusion models,” *arXiv:2303.14795*, Jun. 2023. [Online]. Available: <https://arxiv.org/abs/2303.14795>.
- [9] L. Yang, et al., “Diffusion models: A comprehensive survey of methods and applications,” *arXiv:2209.00796*, Mar. 2023. [Online]. Available: <https://arxiv.org/abs/2209.00796>.
- [10] Y. Liu, H. Du, D. Niyato, J. Kang, Z. Xiong, D. I. Kim, A. Jamalipour, “Deep generative model and its applications in efficient wireless network management: A tutorial and case study,” *arXiv preprint arXiv:2303.17114*, Mar. 2023.
- [11] M. Kim, R. Fritschek, and R. F. Schaefer, “Learning end-to-end channel coding with diffusion models,” *26th International ITG Workshop on Smart Antennas and 13th Conference on Systems, Communications, and Coding (WSA & SCC 2023)*, Braunschweig, Germany, Feb. 27 – Mar. 3, 2023, pp. 1–6.
- [12] M. Arvinte and J. I. Tamir, “MIMO channel estimation using score-based generative models,” *IEEE Trans. Wireless Commun.*, vol. 22, no. 6, pp. 3698–3713, Jun. 2023.
- [13] M. Arvinte and J. I. Tamir, “Score-based generative models for robust channel estimation,” *2022 IEEE Wireless Communications and Networking Conference (WCNC)*, Austin, TX, USA, 2022, pp. 453–458.
- [14] X. Niu, X. Wang, D. Gündüz, B. Bai, W. Chen, and G. Zhou, “A hybrid wireless image transmission scheme with diffusion,” *arXiv preprint arXiv:2308.08244*, Aug. 2023.
- [15] M. Letafati, S. Ali, M. Latva-aho, “Probabilistic constellation shaping with denoising diffusion probabilistic models: A novel approach,” *arXiv preprint arXiv:2309.08688*, Sep. 2023.
- [16] T. Wu, Z. Chen, D. He, L. Qian, Y. Xu, M. Tao, W. Zhang, “CDDM: Channel denoising diffusion models for wireless communications,” *arXiv preprint arXiv:2305.09161*, May 2023.
- [17] G. Lin, A. Milan, C. Shen, and I. Reid, “RefineNet: Multi-path refinement networks for high-resolution semantic segmentation,” in *Proc. IEEE Conf. Comput. Vis. Pattern Recognit. (CVPR)*, Jul. 2017, pp. 1925–1934.
- [18] J. Sohl-Dickstein, E. Weiss, N. Maheswaranathan, and S. Ganguli, “Deep unsupervised learning using nonequilibrium thermodynamics,” *Proceedings of the 32nd International Conference on Machine Learning*, Francis R. Bach and David M. Blei (Eds.), Lille, France, Jul. 2015, vol. 37, pp. 2256–2265.
- [19] Y. Song and S. Ermon, “Generative modeling by estimating gradients of the data distribution,” *Advances in Neural Information Processing Systems 32 (NeurIPS 2019)*, Vancouver, Canada, 2019, vol. 32, pp. 11895–11907.
- [20] F. A. Aoudia and J. Hoydis, “Model-free training of end-to-end communication systems,” *IEEE Journal on Selected Areas in Communications*, vol. 37, no. 11, pp. 2503–2516, Nov. 2019.
- [21] D. P. Kingma, T. Salimans, and M. Welling, “Variational dropout and the local reparameterization trick,” *Advances in Neural Information Processing Systems (NIPS 2015)*, vol. 28, 2015.
- [22] J. Hoydis, S. Cammerer, F. A. Aoudia, A. Vem, N. Binder, G. Marcus, and A. Keller, “Sionna: An open-source library for next-generation physical layer research,” *arXiv preprint arXiv:2203.11854*, Mar. 2023.
- [23] E. Björnson, J. Hoydis, M. Kountouris, and M. Debbah, “Massive MIMO systems with non-ideal hardware: Energy efficiency, estimation, and capacity limits,” *IEEE Transactions on Information Theory*, vol. 60, no. 11, pp. 7112–7139, Nov. 2014.
- [24] Y. Song and S. Ermon, “Improved techniques for training score-based generative models,” *Advances in Neural Information Processing Systems 33 (NeurIPS 2020)*, Dec. 2020.
- [25] C. Beckham and C. Pal, “Conservative objective models are a special kind of contrastive divergence-based energy model,” *arXiv preprint arXiv:2304.03866*, Apr. 2023.
- [26] E. Björnson, M. Matthaiou, and M. Debbah, “A new look at dual-hop relaying: Performance limits with hardware impairments,” *IEEE Transactions on Communications*, vol. 61, no. 11, pp. 4512–4525, Nov. 2013.
- [27] S. A. A. Kalkhoran, M. Letafati, E. Erdemir, B. H. Khalaj, H. Behrooz, and D. Gündüz, “Secure deep-JSCC against multiple eavesdroppers,” *arXiv:2308.02892*, Aug. 2023. [Online]. Available: <https://arxiv.org/abs/2308.02892>.
- [28] 3GPP TSG RAN WG1 #114, R1-2306832, “Evaluation on AI/ML for CSI feedback enhancement,” Meeting #114, Toulouse, France, Tech. Rep., 21st August – 25th August 2023.
- [29] M. Letafati and S. Otoum, “On the privacy and security for e-health services in the metaverse: An overview,” *Ad Hoc Networks*, vol. 150, Nov. 2023, <https://doi.org/10.1016/j.adhoc.2023.103262>.
- [30] M. Letafati and S. Otoum, “Digital healthcare in the metaverse: Insights into privacy and security,” *arXiv:2308.04438v2*, Aug. 2023. [Online]. Available: <https://arxiv.org/abs/2308.04438v2>.
- [31] M. Letafati and S. Otoum, “Global differential privacy for distributed metaverse healthcare systems,” *arXiv:2308.04439*, Jul. 2023. [Online]. Available: <https://arxiv.org/abs/2308.04439>.